Letter | Editors' Suggestion

Atomic-scale Dzyaloshinskii-Moriya-modified Yoshimori spirals in an Fe double layer on Ir(110)

Timo Knispel,[1] Vasily Tseplyaev,[2,3,4] Gustav Bihlmayer,[2,4] Stefan Blügel,[2,3,4] Thomas Michely,[1] and Jeison Fischer[1,*]

[1]*II. Physikalisches Institut, Universität zu Köln, Zülpicher Straße 77, D-50937 Köln, Germany*

[2]*Peter Grünberg Institut, Forschungszentrum Jülich, D-52425 Jülich, Germany*

[3]*Physics Department, RWTH-Aachen University, D-52062 Aachen, Germany*

[4]*Jülich Aachen Research Alliance, D-52425 Jülich, Germany*

(Received 14 November 2024; revised 9 December 2024; accepted 11 December 2024; published 14 January 2025)

Ultrathin magnetic films on heavy metal substrates with strong spin-orbit coupling provide versatile platforms for exploring novel spin textures. So far, structurally open fcc(110) substrates remain largely unexplored. Here, we stabilize a metastable, unreconstructed Ir(110)-(1 × 1) surface on which Fe forms a stable pseudomorphic double layer. Combining spin-polarized scanning tunneling microscopy and *ab initio* calculations, we reveal a right-handed Néel-type spin spiral along the $[\bar{1}10]$ crystallographic direction with a period of 1.27 nm as the magnetic ground state. Our analysis reveals this spiral is of the Yoshimori type, i.e., driven by frustrated Heisenberg interactions, with the Dzyaloshinskii-Moriya interaction determining its cycloidal nature and handedness.

DOI: 10.1103/PhysRevB.111.L020405

Introduction. Ultrathin magnetic films on heavy transition-metal substrates with strong spin-orbit coupling (SOC) have catalyzed breakthroughs in modern condensed matter physics. Landmark studies have revealed interface-induced Dzyaloshinskii-Moriya interactions (DMIs), first demonstrated in a monolayer (ML) of Mn on W(110) [1], have enabled the first observation of atomic-scale skyrmion lattices found in a single ML of Fe/Ir(111) [2], and the first realization of isolated atomic-scale skyrmions in a PdFe bilayer on Ir(111) [3]. In general, one can say that these systems provide a rich landscape for exploring complex, exotic spin textures [4–10] with nonzero vector or scalar spin chiralities, topological phenomena, and their manipulation [3,11] driven by the interplay of reduced dimensionality, surface orientation, stacking sequence, magnetic Heisenberg and beyond-Heisenberg exchange interactions, and the Dzyaloshinskii-Moriya interaction, due to substantial spin-orbit effects in structure inversion-asymmetric environments. Since these platforms are frequently replicated as multilayers [12], they have not only opened new avenues in the study of magnetism, but have also enabled potential applications in spintronics and information technologies [13–16].

Among the ultrathin magnetic film systems, Fe/Ir occupies a distinctive role. It has revealed the crucial role of interactions beyond the Heisenberg model, including four-spin [2] and four-spin–three-site interactions, particularly in bilayer hcp-Rh/Fe/Ir(111) [8] and isoelectronic Rh(111) substrates [9]. These interactions give rise to exotic spin configurations, such as a ground-state square skyrmion lattice or an antiferromagnetic (AFM) up-up-down-down state. Besides studies on (111)-oriented interfaces, (100)-oriented Ir interfaces have also been investigated. For instance, the occurrence of an atomic-scale chiral spin spiral in finite individual bi-atomic Fe chains on the (5 × 1)-Ir(001) surface [6] has been demonstrated, showcasing the diversity of spin textures across different orientations of Ir substrates. It can be summarized that the magnetic structures of Fe on the different Ir substrates can be understood through a competition between ferromagnetic (FM) Heisenberg exchange, beyond-Heisenberg, and Dzyaloshinskii-Moriya interactions.

Despite the impact of the Ir substrate to exciting spin textures, studies focused on the specific Ir(110) substrate are currently lacking. In general, fcc(110) surfaces are of particular interest because their open structure facilitates functionalization and enables tuning of the electronic and magnetic properties in magnetic films. Owing to their C_{2v} symmetry, fcc(110) surfaces can also develop an anisotropic interfacial DMI [17–19], which is essential for stabilizing elliptical skyrmions or antiskyrmions [17]. Together with the inherent anisotropic Heisenberg interaction, they may allow to minimize the skyrmion Hall angle or support the coexistence of skyrmions and antiskyrmions with equal energy, making them promising candidates for racetrack memory devices [20–23].

Experimental results. Despite the potential of fcc(110) surfaces, their preparation is complicated by the complex surface reconstructions observed in spin-orbit materials such as Ir, Pt, and Au [24–29]. To overcome this challenge we prepared a metastable unreconstructed surface of Ir. Cooling Ir(110) from 1200 K in oxygen prevents its nanofacet reconstruction [24,25] through O adsorption. The adsorbed oxygen is subsequently titrated away with H at 470 K. The resulting Ir(110)-(1 × 1) remains thermally stable up to 520 K. The measurements were performed in an ultrahigh vacuum scanning tunneling microscope (STM) operating at 4.2 K and equipped with a vector magnetic field up to 9 T (out of plane) and 2 T in any direction. Spin-polarized STM tips were prepared by coating a W tip with Fe. For more details on experimental methods and sample preparation, see Note 1 in the Supplemental Material (SM) [30].

*Contact author: jfischer@ph2.uni-koeln.de

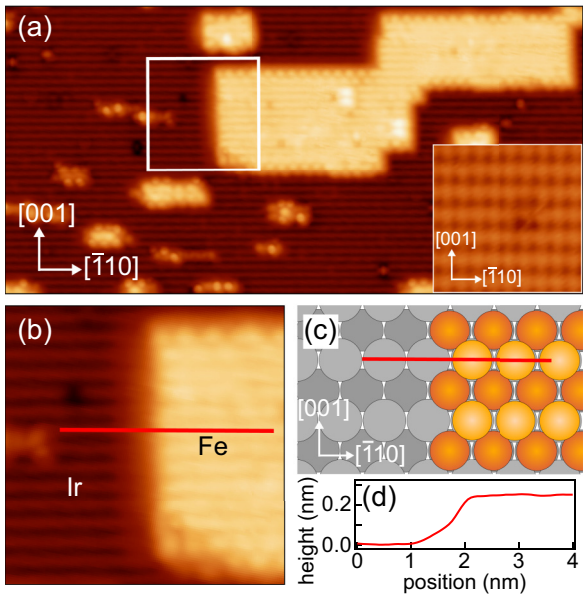

FIG. 1. 2-ML-thick Fe islands on unreconstructed Ir(110)-(1 × 1). (a) Constant-current STM image taken with a nonmagnetic tip after deposition of 0.4 ML Fe on Ir(110)-(1 × 1). $V_b = 100$ mV, $I_{set} = 1$ nA, and image size 28 nm × 14 nm. Inset: Atomically resolved Ir(110)-(1 × 1). $V_b = 50$ mV, $I_{set} = 30$ nA, and image size 3 nm × 3 nm. (b) Zoomed area indicated in (a) by the white square. (c) Top view ball model of Ir(110)-(1 × 1) with a pseudomorphic Fe island on the right (Ir: gray; Fe: orange). (d) STM height profile along the red line in (b).

An STM topograph of Ir(110)-(1 × 1) after deposition of 0.4 ML Fe is shown in Fig. 1(a). Fe deposition results in the formation of Fe islands with a height of 2 ML [see Figs. 1(b)–1(d)] featuring lateral sizes on the order of 10 nm along with smaller Fe islands. While occasionally short isolated strings of Fe atoms in the [$\bar{1}$10] grooves are visible in the frozen state, extended monolayer islands are absent. Fe atoms of neighboring strings are not in direct contact, thus presumably with a negligible interaction. Thereby, the extension of monolayer Fe in the [100] direction is impeded without a stabilizing second Fe layer at the growth temperature. The densely packed atomic rows of bare Ir(110)-(1 × 1) along [$\bar{1}$10] align with those of the 2 ML Fe island [compare Figs. 1(b) and 1(c)], consistent with pseudomorphic growth of the first two Fe layers. The apparent height of the Fe islands, derived from profiles such as in Fig. 1(d), is 0.26 nm, closely matching expectations for pseudomorphic growth and slightly below the 0.27 nm height observed for two Ir layers on Ir(110). For larger deposited amounts pseudomorphic double-layer growth continues up to near complete coverage. A third psudomorphic layer does not form, but by continued Fe deposition instead tall islands nucleate which are presumably composed of bcc Fe.

Spin-polarized STM measurements were conducted with a magnetically soft Fe-coated W tip (for details, see SM [30]). The tip magnetization $\mathbf{m}_{tip}$ aligns to the direction of an external magnetic field $\mathbf{B}$, and enables the decoding of the spin texture within the Fe film, as shown in Fig. 2. The topograph of Fig. 2(a) with $\mathbf{B}$ and thus $\mathbf{m}_{tip}$ normal to the surface reveals a magnetic stripe pattern in the Fe film with a wave vector along [$\bar{1}$10], i.e., along the close packed row direction. The differential conductance (dI/dV) map in Fig. 2(b), taken within the black rectangle depicted in Fig. 2(a), displays the same spin-dependent modulation pattern. The brighter and darker stripes can be straightforwardly interpreted to result from the Fe spin component parallel or antiparallel to the tip magnetization, according to $dI/dV \propto \mathbf{m}_s \cdot \mathbf{m}_{tip}$ with $\mathbf{m}_s$ being the local sample magnetization [36]. Additional information on bias-dependent magnetic contrast is provided in Note 2 in the SM [30]. The average wavelength λ of the magnetic pattern is $\lambda_{expt} = 1.27 \pm 0.02$ nm, fairly independent of island size or shape. With $a_{nn} = 0.2715$ nm being the atomic spacing along the wave vector direction of the magnetic pattern, the wavelength $\lambda = 4.69 a_{nn}$ is incommensurate with respect to the crystal lattice periodicity. Support for the incommensurability of the magnetic pattern with the atomic lattice is given by the spin-resolved and atomically resolved inset of Fig. 2(a), as the spin contrast maxima do not match to a specific position in the atomic lattice defined by the bright protrusions.

To verify the stability of the magnetic pattern, we ramped the out-of-plane field from 1 to 9 T, as shown in Figs. 3(a) and 3(b). The stripe pattern period and intensity remains unchanged up to 9 T, which is even more evident when examining the line profiles in Fig. 3(c). This reveals that $\mathbf{m}_s$ is unaffected by the field, characterizing a hard magnetic sample texture.

To fully characterize the magnetic texture, we probe other spin components by aligning the tip magnetization direction ($\mathbf{m}_{tip}$) along the two orthogonal in-plane directions of the sample using a triple-axes vector magnet [37]. Figures 2(c)–2(g) show dI/dV maps obtained with $B = 1$ T in the following directions: in plane along the [$\bar{1}$10] direction in Fig. 2(c), along the [001] direction in Fig. 2(d), out of plane along the [$\bar{1}\bar{1}$0] direction in Fig. 2(e), along the [1$\bar{1}$0] direction in Fig. 2(f), and finally along the [00$\bar{1}$] direction in Fig. 2(g). The contrast inversion of Fig. 2(e) with respect to Fig. 2(b)—easy to spot with the help of the vertical white line marking a defect (bright bump, marked by white vertical line), unaffected by the tip magnetization or external magnetic field—confirms that $\mathbf{m}_{tip}$ follows the direction of the external $\mathbf{B}$. It is obvious from the dI/dV maps, that besides spin components normal to the surface [Figs. 2(b) and 2(e)], the texture displays also spin components parallel to the wave vector of the pattern [Figs. 2(c) and 2(f)], but no in-plane spin components normal to the wave vector [Figs. 2(d) and 2(g)]. These spin components are consistent with a flat Néel or cycloidal spiral, but inconsistent with a Bloch spiral.

The handedness of the Néel spiral is evaluated analyzing dI/dV line profiles represented in Fig. 2(h). The line profiles are averages along the lines in Figs. 2(b)–2(d). They are aligned with the help of the defect. Turning the tip magnetization from normal [black curve, Fig. 2(b)] into the surface along the wave vector of the magnetic pattern [red curve, Fig. 2(c)] leads to a shift of the stripe pattern by about $\frac{1}{4}\lambda$ into [$\bar{1}$10] as visible in Fig. 2(h), defining a clockwise or right-handed rotation of the spin texture ($\downarrow \leftarrow \uparrow \rightarrow \downarrow$). Similar analyses for other islands unequivocally support a unique rotational sense. To conclude, 2 ML Fe on Ir(110) displays

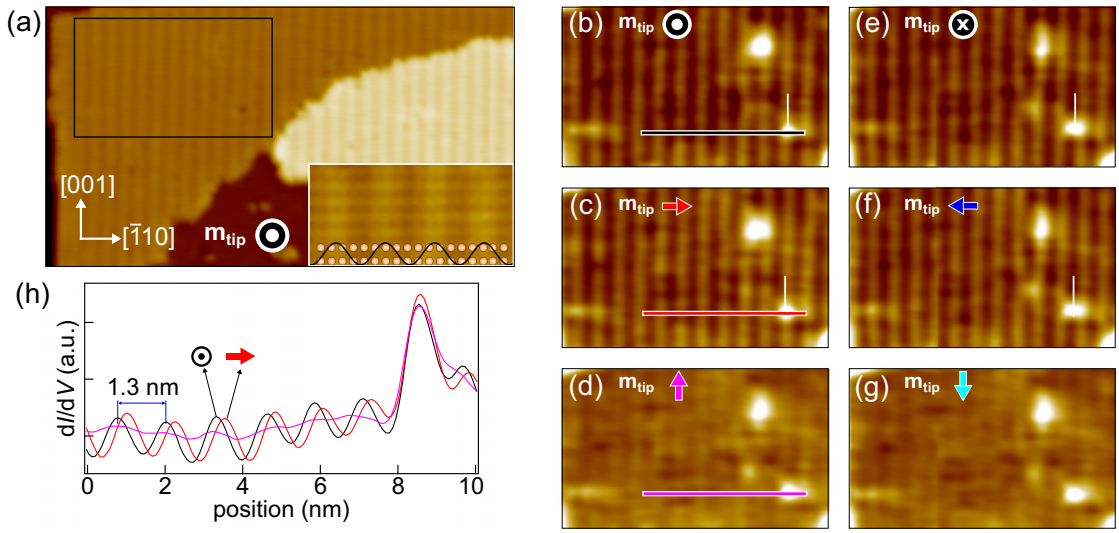

FIG. 2. Spin-polarized STM data obtained using a magnetically soft Fe-coated W tip with magnetization $\mathbf{m}_{tip}$ whose indicated direction is the one of the external field $B = 1$ T. (a) Spin-polarized STM topograph of 2 ML Fe on Ir(110) with a substrate step crossing from the lower left to the upper right. Only the area in the lower center is not covered by Fe. A magnetic stripe pattern of the out-of-plane magnetization direction with a wave vector in the [$\bar{1}$10] direction is visible in 2 ML Fe areas. $V_b = 100$ mV, $I_{set} = 5$ nA, and the image size is 38 nm × 20 nm. Inset: Spin-resolved and atomically resolved STM topograph. Circles are superimposed at locations of atomic intensity maxima in the lower part of the image. The magnetic stripe pattern schematically represented by a sinusoidal curve is incommensurate with atomic positions. $V_b = 50$ mV, $I_{set} = 1$ nA, and the image size is 5.0 nm × 2.5 nm. (b)–(g) Spin-polarized dI/dV maps taken at indicated $\mathbf{m}_{tip}$ defined by an external field. Magnetic contrast is observed for $\mathbf{m}_{tip}$ normal to the surface in (b) and (e) as well as along or opposite to [$\bar{1}$10] in (c) and (f). The magnetic contrast vanishes in (d) and (g) for $\mathbf{m}_{tip}$ along or opposite to [001], i.e., for $\mathbf{m}_{tip}$ normal to the pattern wave vector. $V_b = 100$ mV, $I_{set} = 5$ nA, and the image size is 16 nm × 10 nm. (h) Averaged dI/dV profiles for colored linelike rectangles in (b)–(d) (colors matched). The profiles are taken with respect to a defect marked by vertical white lines in (b)–(d) as reference.

a clockwise rotating cycloidal or Néel-type spin spiral with a wavelength of $\lambda = 4.69a_{nn}$. It is incommensurate to the underlying crystal lattice and magnetically hard with no changes in spin texture up to 9 T.

Theoretical results. To investigate the physical origin of the robust spin spiral, we performed vector-spin density functional theory (DFT) calculations using the film version of the full-potential linearized augmented plane-wave method [38] (FLAPW) as implemented in the FLEUR code [39] to analyze their energetics in a structurally optimized pseudomorphic, two-layer Fe film on an 11-layer Ir substrate modeling the experimental sample. The local density approximation (LDA) [40] was applied, resulting in an optimized lattice constant of $a_0 = 0.382$ nm, in good agreement with experiment (0.3839 nm). The structural optimization of the film includes the first four layers of the system with relaxations of -19%, -7%, -1% of the first and second Fe layer and first Ir layer in units of the interlayer distance in the [110] direction, $a_0/\sqrt{8}$. The calculations of homogeneous spin spirals have been performed in the $p(1 \times 1)$ unit cell, exploiting the generalized Bloch theorem [41] for calculations without SOC. The contribution of SOC to the spirals has been treated in first-order perturbation theory [42]. Here, 3840 $\mathbf{k}_{\parallel}$ points in the two-dimensional Brillouin zone have been used.

The DFT results are summarized in Fig. 4. Calculations without SOC reveal a spin spiral with a symmetric ($\mathbf{q} \leftrightarrow -\mathbf{q}$) dispersion featuring two deep energy minima (<-10 meV below the FM state) at finite, accidental, i.e., not symmetry determined values of $\pm q$, with $q_{[\bar{1}10]} = 0.194(\frac{2\pi}{a})$, along the high-symmetry line [$\bar{1}$10]. This corresponds to an atomic-scale spin-spiral period of $\lambda_{theo} = 1.39$ nm. The solution is an example of the well-known Yoshimori spiral [43] resulting from frustrated exchange, arising from competing FM and AFM Heisenberg interactions between different pairs of atoms [44].

When SOC is included, (i) the magnetocrystalline anisotropy (MCA) is determined and we theoretically confirm the easy axis of magnetization orients along the out-of-plane direction, the medium ($E_{[\bar{1}10]} - E_{[110]} = 0.32$ meV/Fe) and hard axes ($E_{[001]} - E_{[110]} = 1.18$ meV/Fe) are along the [$\bar{1}$10] and [001] directions, respectively. (ii) For a cycloidal Néel-type spiral, the associated DMI lifts the energetic degeneracy by ± 2 meV, the minima become asymmetric, favoring energetically a chiral ground-state Néel spiral with a positive q value, i.e., a clockwise rotating spiral, though the DMI does not significantly alter the position of the energy minimum. The energy gain of 10.4 meV/Fe from spiral formation significantly exceeds the average MCA contribution of 0.16 meV/Fe along the spiral. Thus, the MCA has a negligible impact on the spiral configuration, and a homogeneous spiral is expected. Along the [001] direction, a different scenario is observed: Without SOC, no Yoshimori spiral is observed, the FM state has the lowest energy, but the DMI selects a positive $q_{[001]} = 0.14(\frac{2\pi}{a})$ corresponding to $\lambda_{[001]} = 2.08$ nm, though at higher energy than for the [$\bar{1}$10] direction. Consequently, a ground-state spin spiral stabilizing along [001] is less favorable.

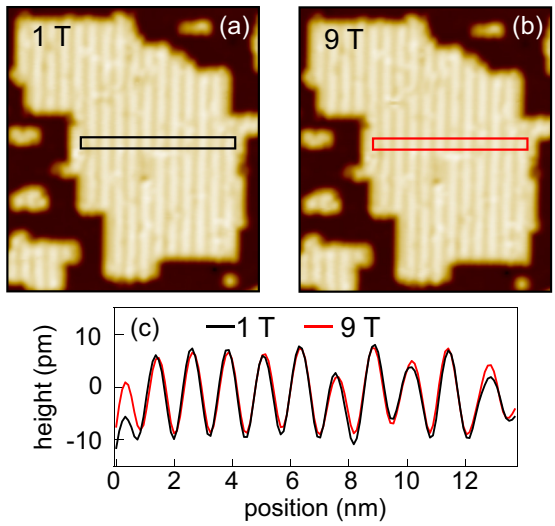

FIG. 3. Stability of frustrated spin spiral against a high magnetic field. Spin-polarized STM images of 2 ML Fe islands on Ir(110) at an external out-of-plane magnetic field of (a) 1 T and (b) 9 T ($V_b = 100$ mV, $I_{set} = 1$ nA, 23 nm × 26 nm, and $T = 4.2$ K). (c) Comparison of line profiles averaged over lines within the rectangle in (a) and (b). The modulation pattern is unchanged and sinusoidal behavior is present in both cases.

Discussion. Comparing theory with experiment, we conclude the following: (i) The direction of the spiral agrees, (ii) the sign of the q vector and thus the handedness of the spiral agrees, and (iii) there is a good agreement between the periods determined by theory and experiment, $\lambda_{theo} = 1.39$ nm vs $\lambda_{expt} = 1.27 \pm 0.02$ nm. Turning to the analysis of the energy, we map the dispersion without SOC to a classical Heisenberg model $E = -\sum_i J_{0i} S^2 \hat{\mathbf{e}}_0 \cdot \hat{\mathbf{e}}_i$, with $\hat{\mathbf{e}}$ being the direction vectors of the local spin. We notice that the frustration of the Heisenberg exchange between the FM interaction of interplane nearest-neighbor pairs and the AFM pair interaction of intraplane more-distant neighbors (for calculated exchange constants, see Note 3 in the SM [30]) is five times stronger than the relativistic DMI. Thus, the frustrated exchange determines the energy and length scale of the spiral, but the DMI selects of the many possible spirals the clockwise rotating Néel-type one. Finally, the energy minimum is about 12 meV/Fe atom below the FM state, suggesting that an external magnetic field of around 80 T would be required to unwind it into a skyrmion texture. This is consistent with the observed stability up to the highest applied field of 9 T.

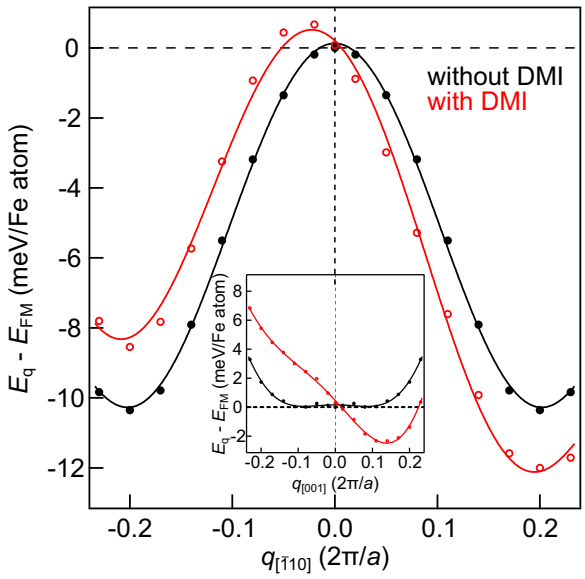

FIG. 4. DFT calculated energy dispersions $E(q)$ relative to the FM state of homogeneous, flat cycloidal spin spirals as a function of the wave vector q for 2 ML Fe/Ir(110). Films with (red) and without (black) DMI along two orthogonal propagation directions: $[\bar{1}10]$ (main plot) and [001] (inset). Positive (negative) q indicates a right- (left-)handed rotational sense. Solid lines are polynomial fits to the data point closely matching the points up to the Brillouin zone boundary (not shown).

Mapping the energy dispersions around $q = 0$ to a micromagnetic model in which the strength of the Heisenberg exchange is expressed by the spin stiffness A in $E(q) = Aq^2$ and the strength of the DMI by the spiralization D in $E(q) = Dq$, we find a strong asymmetry of the exchange interaction in different directions, $A_{[\bar{1}10]} = -19.8$ meV (as the minus sign implies, the FM state is not stable), and $A_{[001]} = -0.1$ meV, while the spiralization is fairly isotropic $D_{[\bar{1}10]} = -5.2$ meV/nm, and $D_{[001]} = -5.0$ meV/nm, with the same handedness in both directions.

Summary. In summary, we find that the magnetic ground state of pseudomorphic double-layer Fe islands on unreconstructed Ir(110) is a frozen clockwise Néel-type atomic-scale cycloidal spin spiral along the $[\bar{1}10]$ direction with a wavelength of 1.27 nm. This spin spiral exhibits a large magnetic stiffness, remaining stable under external fields up to 9 T. DFT calculations show that, unlike (111) and (100) Ir substrates, the spin spiral here is of Yoshimori type, caused by frustrated Heisenberg exchange interactions, with the Dzyaloshinskii-Moriya interaction favoring a Néel over a Bloch spiral and breaking the chiral symmetry that determines its unique handedness. The exchange interaction is highly anisotropic, while the micromagnetically averaged DMI is relatively isotropic, and no significant beyond-Heisenberg interactions were observed. These findings provide new insights into stabilizing atomic-scale spin spirals on low-symmetry substrates, highlighting the role of anisotropic magnetic interactions in determining the ground state. Future work could explore tuning spin textures through surface modifications, leveraging the openness of fcc(110) substrates.

Acknowledgments. V.T. and S.B. thank Markus Hoffmann for his support in carrying out the DFT calculations. We acknowledge funding from Deutsche Forschungsgemeinschaft (DFG) through CRC 1238 Grant No. 277146847, projects B06 and C01. S.B. and J.F. acknowledge financial support from DFG through projects BL 444/16-2 and FI 2624/1-1 within the SPP 2137 (Grant No. 462692705). S.B. acknowledges financial support from the European Research Council (ERC) under the European Union's Horizon2020 research and innovation program (Grant No. 856538, project "3D MAGiC"). G.B. gratefully acknowledges computing time granted through JARA-HPC on the supercomputer JURECA at Forschungszentrum Jülich.

[1] M. Bode, M. Heide, K. von Bergmann, P. Ferriani, S. Heinze, G. Bihlmayer, A. Kubetzka, O. Pietzsch, S. Blügel, and R. Wiesendanger, Chiral magnetic order at surfaces driven by inversion asymmetry, Nature (London) **447**, 190 (2007).

[2] S. Heinze, K. von Bergmann, M. Menzel, J. Brede, A. Kubetzka, R. Wiesendanger, G. Bihlmayer, and S. Blügel, Spontaneous atomic-scale magnetic skyrmion lattice in two dimensions, Nat. Phys. **7**, 713 (2011).

[3] N. Romming, C. Hanneken, M. Menzel, J. E. Bickel, B. Wolter, K. von Bergmann, A. Kubetzka, and R. Wiesendanger, Writing and deleting single magnetic skyrmions, Science **341**, 636 (2013).

[4] P. Ferriani, K. von Bergmann, E. Y. Vedmedenko, S. Heinze, M. Bode, M. Heide, G. Bihlmayer, S. Blügel, and R. Wiesendanger, Atomic-scale spin spiral with a unique rotational sense: Mn monolayer on W(001), Phys. Rev. Lett. **101**, 027201 (2008).

[5] Y. Yoshida, S. Schröder, P. Ferriani, D. Serrate, A. Kubetzka, K. von Bergmann, S. Heinze, and R. Wiesendanger, Conical spin-spiral state in an ultrathin film driven by higher-order spin interactions, Phys. Rev. Lett. **108**, 087205 (2012).

[6] M. Menzel, Y. Mokrousov, R. Wieser, J. E. Bickel, E. Vedmedenko, S. Blügel, S. Heinze, K. von Bergmann, A. Kubetzka, and R. Wiesendanger, Information transfer by vector spin chirality in finite magnetic chains, Phys. Rev. Lett. **108**, 197204 (2012).

[7] M. Hervé, B. Dupé, R. Lopes, M. Böttcher, M. D. Martins, T. Balashov, L. Gerhard, J. Sinova, and W. Wulfhekel, Stabilizing spin spirals and isolated skyrmions at low magnetic field exploiting vanishing magnetic anisotropy, Nat. Commun. **9**, 1015 (2018).

[8] N. Romming, H. Pralow, A. Kubetzka, M. Hoffmann, S. von Malottki, S. Meyer, B. Dupé, R. Wiesendanger, K. von Bergmann, and S. Heinze, Competition of Dzyaloshinskii-Moriya and higher-order exchange interactions in Rh/Fe atomic bilayers on Ir(111), Phys. Rev. Lett. **120**, 207201 (2018).

[9] A. Krönlein, M. Schmitt, M. Hoffmann, J. Kemmer, N. Seubert, M. Vogt, J. Küspert, M. Böhme, B. Alonazi, J. Kügel, H. A. Albrithen, M. Bode, G. Bihlmayer, and S. Blügel, Magnetic ground state stabilized by three-site interactions: Fe/Rh (111), Phys. Rev. Lett. **120**, 207202 (2018).

[10] J. Spethmann, S. Meyer, K. von Bergmann, R. Wiesendanger, S. Heinze, and A. Kubetzka, Discovery of magnetic single- and triple-**q** states in Mn/Re (0001), Phys. Rev. Lett. **124**, 227203 (2020).

[11] S. Krause and R. Wiesendanger, Skyrmionics gets hot, Nat. Mater. **15**, 493 (2016).

[12] C. Moreau-Luchaire, C. Moutafis, N. Reyren, J. Sampaio, C. A.F. Vaz, N. Van Horne, K. Bouzehouane, K. Garcia, C. Deranlot, P. Warnicke, P. Wohlhüter, J. M. George, M. Weigand, J. Raabe, V. Cros, and A. Fert, Additive interfacial chiral interaction in multilayers for stabilization of small individual skyrmions at room temperature, Nat. Nanotechnol. **11**, 444 (2016).

[13] J. Sampaio, V. Cros, S. Rohart, A. Thiaville, and A. Fert, Nucleation, stability and current-induced motion of isolated magnetic skyrmions in nanostructures, Nat. Nanotechnol. **8**, 839 (2013).

[14] K. M. Song, J.-S. Jeong, B. Pan, X. Zhang, J. Xia, S. Cha, T.-E. Park, K. Kim, S. Finizio, J. Raabe, J. Chang, Y. Zhou, W. Zhao, W. Kang, H. Ju, and S. Woo, Skyrmion-based artificial synapses for neuromorphic computing, Nat. Electron. **3**, 148 (2020).

[15] S. H. Yang, R. Naaman, Y. Paltiel, and S. Parkin, Chiral spintronics, Nat. Rev. Phys. **3**, 328 (2021).

[16] K. Everschor-Sitte, A. Majumdar, K. Wolk, and D. Meier, Topological magnetic and ferroelectric systems for reservoir computing, Nat. Rev. Phys. **6**, 455 (2024).

[17] M. Hoffmann, B. Zimmermann, G. P. Müller, D. Schürhoff, N. S. Kiselev, C. Melcher, and S. Blügel, Antiskyrmions stabilized at interfaces by anisotropic Dzyaloshinskii-Moriya interactions, Nat. Commun. **8**, 308 (2017).

[18] L. Camosi, S. Rohart, O. Fruchart, S. Pizzini, M. Belmeguenai, Y. Roussigné, A. Stashkevich, S. M. Cherif, L. Ranno, M. de Santis, and J. Vogel, Anisotropic Dzyaloshinskii-Moriya interaction in ultrathin epitaxial Au/Co/W(110), Phys. Rev. B **95** 214422 (2017).

[19] C. Q. Liu, Y. B. Zhang, G. Z. Chai, and Y. Z. Wu, Large anisotropic Dzyaloshinskii-Moriya interaction in CoFeB(211)/Pt(110) films, Appl. Phys. Lett. **118**, 262410 (2021).

[20] S. Huang, C. Zhou, G. Chen, H. Shen, A. K. Schmid, K. Liu, and Y. Wu, Stabilization and current-induced motion of antiskyrmion in the presence of anisotropic Dzyaloshinskii-Moriya interaction, Phys. Rev. B **96**, 144412 (2017).

[21] J. Xia, X. Zhang, M. Ezawa, Q. Shao, X. Liu, and Y. Zhou, Dynamics of an elliptical ferromagnetic skyrmion driven by the spin-orbit torque, Appl. Phys. Lett. **116**, 022407 (2020).

[22] C. Cheng, Z. Yan, J. Dong, Y. Liu, Z. Xia, L. Li, and X. Han, Elliptical skyrmion moving along a track without transverse speed, Phys. Rev. B **104**, 174409 (2021).

[23] M. Hoffmann, G. P. Müller, C. Melcher, and S. Blügel, Skyrmion-antiskyrmion racetrack memory in rank-one DMI materials, Front. Phys. **9**, 769873 (2021).

[24] R. Koch, M. Borbonus, O. Haase, and K. H. Rieder, New aspects on the Ir(110) reconstruction: Surface stabilization on mesoscopic scale via (331) facets, Phys. Rev. Lett. **67**, 3416 (1991).

[25] J. J. Schulz, M. Sturmat, and R. Koch, Illuminating structural transformation of Ir(110): A high-temperature scanning tunneling microscopy study, Phys. Rev. B **62**, 15402 (2000).

[26] H. Niehus, Analysis of the Pt(110)-(1 × 2) surface reconstruction, Surf. Sci. **145**, 407 (1984).

[27] T. Gritsch, D. Coulman, R. J. Behm, and G. Ertl, A scanning tunneling microscopy investigation of the structure of the Pt(110) and Au(110) surfaces, Surf. Sci. **257**, 297 (1991).

[28] I. K. Robinson, Direct determination of the Au(110) reconstructed surface by x-ray diffraction, Phys. Rev. Lett. **50**, 1145 (1983).

[29] C. Höfner and J. W. Rabalais, Deconstruction of the Au(110)-(1 × 2) surface, Phys. Rev. B **58**, 9990 (1998).

[30] See Supplemental Material at http://link.aps.org/supplemental/10.1103/PhysRevB.111.L020405 for additional experimental data and supporting theory, which includes Refs. [24,31–35].

[31] A. Ney, J. J. Schulz, M. Sturmat, and R. Koch, Stress-driven self-assembly on Ir(110): Stripes, droplets, and missing-row-type reconstructions, Surf. Sci. **519**, 192 (2002).

[32] C. M. Chan, S. L. Cunningham, K. L. Luke, W. H. Weinberg, and S. P. Withrow, Determination of the atomic arrangement of the unreconstructed Ir(110) surface by low-energy electron diffraction a, Surf. Sci. **78**, 15 (1978).

[33] K. Heinz, G. Schmidt, L. Hammer, and K. Müller, Dynamics of the reconstruction process Ir(100)$1 \times 1 \rightarrow 1 \times 5$, Phys. Rev. B **32**, 6214 (1985).

[34] S.-H. Phark, J. A. Fischer, M. Corbetta, D. Sander, and J. Kirschner, Superparamagnetic response of Fe-coated W tips in spin-polarized scanning tunneling microscopy, Appl. Phys. Lett. **103**, 032407 (2013).

[35] J. A. Fischer, L. M. Sandratskii, S.-H. Phark, D. Sander, and S. Parkin, Atomic structure governed diversity of exchange-driven spin helices in Fe nanoislands: Experiment and theory, Phys. Rev. B **96**, 140407(R) (2017).

[36] D. Wortmann, S. Heinze, Ph Kurz, G. Bihlmayer, and S. Blügel, Resolving complex atomic-scale spin structures by spin-polarized scanning tunneling microscopy, Phys. Rev. Lett. **86**, 4132 (2001).

[37] S. Meckler, N. Mikuszeit, A. Preßler, E. Y. Vedmedenko, O. Pietzsch, and R. Wiesendanger, Real-space observation of a right-rotating inhomogeneous cycloidal spin spiral by spin-polarized scanning tunneling microscopy in a triple axes vector magnet, Phys. Rev. Lett. **103**, 157201 (2009).

[38] E. Wimmer, H. Krakauer, M. Weinert, and A. J. Freeman, Full-potential self-consistent linearized-augmented-plane-wave method for calculating the electronic structure of molecules and surfaces: O_2 molecule, Phys. Rev. B **24**, 864 (1981).

[39] D. Wortmann, G. Michalicek, N. Baadji, W. Beida, M. Betzinger, G. Bihlmayer, T. Bornhake, J. Bröder, T. Burnus, J. Enkovaara, F. Freimuth, C. Friedrich, C.-R. Gerhorst, S. Granberg Cauchi, U. Grytsiuk, A. Hanke, J.-P. Hanke, M. Heide, S. Heinze, R. Hilgers, H. Janssen, D. A. Klüppelberg *et al.*, FLEUR, doi:10.5281/zenodo.7576163.

[40] S. H. Vosko, L. Wilk, and M. Nusair, Accurate spin-dependent electron liquid correlation energies for local spin density calculations: A critical analysis, Can. J. Phys. **58**, 1200 (1980).

[41] Ph. Kurz, F. Förster, L. Nordström, G. Bihlmayer, and S. Blügel, *Ab initio* treatment of noncollinear magnets with the full-potential linearized augmented plane wave method, Phys. Rev. B **69**, 024415 (2004).

[42] M. Heide, G. Bihlmayer, and S. Blügel, Describing Dzyaloshinskii–Moriya spirals from first principles, Phys. B: Condens. Matter **404**, 2678 (2009).

[43] A. Yoshimori, A new type of antiferromagnetic structure in the rutile type crystal, J. Phys. Soc. Jpn. **14**, 807 (1959).

[44] S. H. Phark, J. A. Fischer, M. Corbetta, D. Sander, K. Nakamura, and J. Kirschner, Reduced-dimensionality-induced helimagnetism in iron nanoislands, Nat. Commun. **5**, 5183 (2014).